Construction and Building Materials 387 (2023) 131587

Contents lists available at ScienceDirect

Construction and Building Materials

journal homepage: www.elsevier.com/locate/conbuildmat

Analysis of the hydraulic performance of permeable pavements on a layer-by-layer basis

Eneko Madrazo-Uribeetxebarria [a,*], Maddi Garmendia Antín [a], Gorka Alberro Eguilegor [a], Ignacio Andrés-Doménech [b]

[a] Faculty of Engineering in Gipuzkoa, University of the Basque Country UPV/EHU, Europa Plaza, 1, Donostia, 20018, Spain
[b] Instituto Universitario de Investigacion de Ingenieria del Agua y del Medio Ambiente (IIAMA), Universitat Politecnica de Valencia, Camino de vera s/n, Valencia, 46022, Spain

ARTICLE INFO

Keywords:
Permeable pavement
Porous asphalt mixture
Permeable interlocking concrete block
SWMM
Low impact development
Model calibration

ABSTRACT

Permeable pavement systems are a sustainable urban drainage technique created with a highly porous base and subbase. This study first analyses the hydraulic performance of several new permeable pavement systems based on 189 experimental hydrographs. In addition, the analysis explores the influence of rain intensity, slope, and, as a novelty, individual layers. Analysed variables were outflow peak, time to peak, and time to specific cumulative discharges. Secondly, based on the experimental hydrographs, the study explores the performance of the permeable pavement module defined in the Storm Water Management Model, carried out in two steps. First, single-layer outflows were used to calibrate parameter values that could not be measured physically, using the differential evolution algorithm and Nash–Sutcliffe model efficiency coefficient as an objective function. Later, complete layout hydrographs were tested without calibration, and model performance was checked. Results show that the superficial permeable interlocking paver layer provides a notably higher retention capacity than the porous asphalt mixture. Individual modelling results show that the soil layer definition is inappropriate for gravel-type layers, even with a geotextile. Despite this, complete section performance is quite good without calibration if the soil layer is not selected on the model. These results are expected to reduce modelling uncertainty, especially when no calibration data is available.

1. Introduction

Green infrastructure, which mimics the natural hydrological cycle, has proven to be an efficient solution to be implemented in urban environments to improve the sustainability of surface water management [1], but also as a mechanism for enhancing resilience to climate change and flooding. Sustainable Urban Drainage System (SUDS) is a more specific term used for designating certain technologies and techniques, which aim to manage stormwater in a more sustainable manner than conventional solutions [2], reducing the soil-sealing effect of urbanisation. One such technique is Permeable Pavement (PP) systems, which, unlike other SUDS techniques, provide a transitable hard surface while managing surface stormwater [3], making it a very advantageous solution for highly urbanised areas. In addition, PP also offers several environmental benefits, such as [4]: runoff volume and peak reduction, enhanced stormwater infiltration into the native soil, water quality improvement, heat-island effect mitigation, and traffic noise reduction.

Compared to traditional pavements, created by laying several granular materials and sealed with an impervious surface, PP systems are created with highly porous base and subbase to enable water infiltration and storage [5]. That porous base is crowned by a transitable surface, also highly porous, which can be monolithic or modular, being the most researched surface materials [6]: Permeable Concrete (PC), Permeable Asphalt mixture (PA), and Permeable Interlocking Paver (PIP).

The hydraulic properties of PP systems are fundamental for their performance as SUDS. Moreover, hydraulic processes are influenced by several sub-surface characteristics, such as layer thickness, pore size, pore distribution, and pore geometry [6]. In that sense, the volume reduction provided by PP systems is highly influenced by surface properties, such as permeability, being the volume reduction higher for PA than for PIP [7]. In the case of newly built PIPs, infiltration capacity is higher than 90% for slopes up to 10%, being higher for lower slopes [8]. The retention capacity of PP systems is also reduced by the creation of preferential paths by PIPs [9]. In that regard, a larger

* Corresponding author.
E-mail address: eneko.madrazo@ehu.eus (E. Madrazo-Uribeetxebarria).

https://doi.org/10.1016/j.conbuildmat.2023.131587
Received 20 March 2023; Received in revised form 23 April 2023; Accepted 27 April 2023

aggregate size used in PP systems tends to reduce horizontal hydraulic conductivity compared to common soils considerably [10].

On the other hand, PP system outflow varies in response to rainfall duration and pavement initial wetting conditions. Alsubih et al. [11] tested the impact of these latter two and found that the outflow duration for all rainfall events and tested conditions was significantly longer than the rainfall duration. Liu and Chui [12] studied how several factors influenced runoff from PP systems, concluding that from the five checked design parameters, storage depth was the most influential factor, followed by the conductivity of the subgrade soil.

However, it is essential to integrate SUDS into the existing stormwater network [13]. For this purpose, mathematical models are a fundamental tool since they facilitate the decision-making process when implementing this type of solution in the urban environment. Nevertheless, further research is needed to improve modelling techniques and properly evaluate SUDS performance [14].

There are several modelling approaches to SUDS; a detailed review can be found in [14]. By extension, various models are also available. However, the Storm Water Management Model (SWMM) is one of the most popular among researchers, thanks to the rich selection of hydrologic and hydraulic computation methods and the free access to the model [15]. Initially, SWMM was developed to assist practitioners in sizing stormwater and grey wastewater infrastructure [16]. However, it has implemented several SUDS models, named Low Impact Development Control (LIDC), including PP.

Being relatively new elements in a widely used model, these LIDC models are still being tested and their performance evaluated. Zhang and Guo [17] tested the PP module in SWMM, comparing it with results from a standard catchment, and concluded that the infiltration rate provided by PP was incomplete, as it should take into account drainage capacity and subbase storage capacity. Randall et al. [18] investigated the long-term performance of three experimental stalls located on a parking site and found that SWMM overestimated evaporation rates on PP. Platz et al. [16] tested the SWMM LIDCs for empirical data from specific PP monitoring and found that SWMM satisfactorily modelled the PP. However, the average predicted peak was 35% lower than the measured one, and modelled average volume was 5% lower. Madrazo-Uribeetxebarria et al. [19] also attempted to check single-event modelling performance on SWMM for PIPs and PA surfaces, finding that peak and volume differences were less than 10%.

Even so, further research is still required. As a preliminary step to deepen the model performance, the authors conducted a sensitivity analysis of the PP model given in SWMM. One of the most relevant conclusions obtained from the analysis was that some parameters could be neglected when the outflow from the PP is modelled. The analysis also pointed out that some parameters are more influential than others, giving an order of priority for parameters according to their influence in the outflow control [20].

Nevertheless, more than one sensitivity analysis is required to reduce modelling uncertainty. Other factors, such as the modeller's limitations in describing the physical reality, also contribute to modelling uncertainty [21]. In that regard, and bearing in mind that the PP model in SWMM is defined on a layer basis, real-life applications usually have a different layer structure than the model. Sometimes because layout includes elements not considered in the model, such as the geotextile between the base layer and the subbase layer, or because the practitioner is not sure if a specific element, the soil layer in SWMM, for example, has to be selected or how to apply it.

In that regard, [22] studied the potential of new a type of PP with micro-detention storage by setting hydrological parameters experimentally and, after calibration, testing the potential of SWMM to model the performance of the new pavement. [23] also compared SWMM modelling capabilities for bioretention systems based on experimental data obtained in the laboratory with constant rainfalls of 15-min duration. Instead, [24] tested the HYDRUS-2D model based on laboratory data and calibrating some parameters. However, no previous study is analysing SWMM on a layer basis.

The global objective of this study is twofold. Firstly, it explores the hydraulic response of new PPs, where clogging has yet to start, in the short term under specific controlled conditions. For that purpose, a novel approach is proposed by testing the PP system layer-by-layer, not just with the complete cross-section. Secondly, the study confronts experimental data with the PP model provided by SWMM, as no previous study is known to validate the capability of SWMM's LIDC module for representing the hydrological performance of a PP system in the short term based on experimental data. The analysis is also carried out layer-by-layer to gain new insight into the model. Although clogging is another factor to be taken into account in the long term, we underline the interest in the initial behaviour of the pavement. Hence, the specific objectives set for the study are: (1) to check how outflow hydrographs are influenced, for complete cross-sections and each layer, by slope, rain, and pavement type, and (2) to test sub-surface hydrograph prediction performance for the model.

For that purpose, the processes are set up as follows: (a) measure drain outflow hydrographs for several PP setups under specific laboratory conditions; (b) set the parameters for modelling, measuring physical parameters, and calibrating, on a layer basis, parameters that cannot be physically measured; (c) compute modelling hydrographs equivalent to those measured under laboratory conditions with previous parameters without calibration; and (d) characterise the modelling performance of SWMM by comparing experimental and modelling results.

Thereby, the article presents, firstly, the materials and methodology used during this study in Section 2. Later, obtained results are presented in Section 3 and discussed in Section 4. All three sections were divided into two, one related to experimental data and another related to modelling data. Finally, conclusions are given in Section 5.

2. Materials and methods

In order to measure outflow hydrographs from several cross-sections under different rain intensities and slopes, 40-min laboratory experiments were conducted. This section describes (2.1) the selected precipitation regime, (2.2) the equipment used to perform mentioned experiments, (2.3) analysed materials and layouts, (2.4) the experimental procedure, (2.5) the selected criteria to analyse experimental hydrographs, and (2.6) how modelling data were obtained and compared. The methodology described in this section is summarised in Fig. 1.

2.1. Climatological data

The study was undertaken with data gathered in Donostia/San Sebastián (Spain), facing the Bay of Biscay in an Atlantic climate. Climatological data was gathered from Igeldo weather station (43°19′0″N, 2°0′0″W), with extensive historical data and average annual rainfall of 1500 mm. Based on IDF curves for the period 1927–2016 [25], 35/70/140 mm/h intensities were selected, named *low/high/extreme*, correspondent to a 2/10/500 return period rainfalls of 15 min duration, which corresponds, for urban watersheds, to the range of the most frequent time of concentrations values until the network inlet [26]. Hence, applied precipitation volumes were 8.75 mm, 17.5 mm, and 35 mm.

2.2. Equipment

Experimental tests were carried out on a GUNT HM-164 hydrological bench. The original bench had a circuit to create artificial rain but was modified to better control flows, create uniform raindrops, and measure outflows. An image of the bench and a diagram of the modified circuit are shown in Fig. 2.

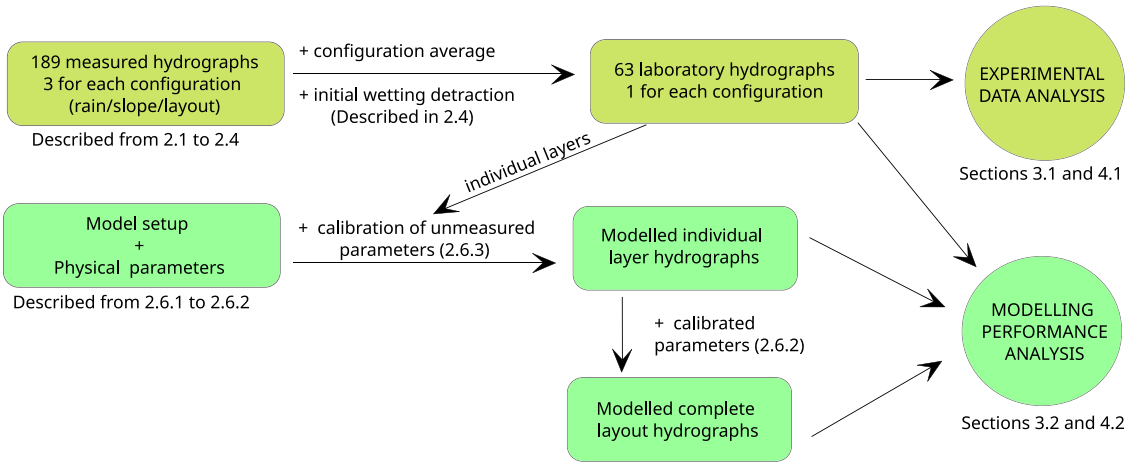

Fig. 1. Flowchart describing the methodology followed to obtain experimental and derived modelling results.

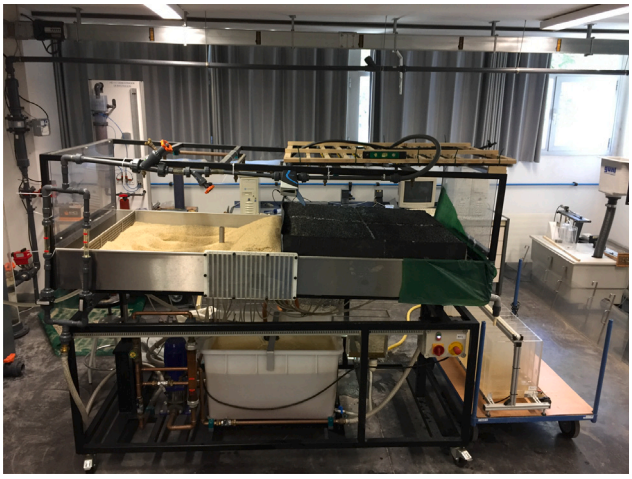

(a) Experimental bank.

(b) Schematic representation of the experimental bank.

Fig. 2. (a) Experimental bank and (b) a diagram with the key components.

The precipitation regime was simulated by a grid of evenly spaced mesh of 81 drippers located in the upper part of the hydrological bank, at a distance of 40 cm to 60 cm, depending on the tested layer. The mesh was kept horizontal during the experiments to ensure uniform dripper discharge. The selected flow was controlled with two rotameters; the first one, rotameter A, had a flow range of 15 to 160 l/h, and the second one, rotameter B, had a range of 5 to 50 l/h. Rotameter A set *high* and *extreme* precipitation regimes, while rotameter B set *low* precipitation. The applied flow was measured by a 15 mm iPerl flowmeter with a graphic display of 1 l/h precision. Flow was controlled by several valves placed along the circuit.

The bench had a platform to lay the material, and a specific slope could be selected. Materials were laid out in half of the test bench, resulting in all analysed cross sections having a surface area of 1.0 m × 1.0 m. All tested materials were laid over an impermeable, smooth surface of waterproofing high-density polyethylene geomembrane laid over the bench platform. Water was drained over the membrane to an outflow pipe, discharging the hydrograph buckets. Thus, outflow from the test bench was collected in 15 identical buckets which an individual capacity of 5700 ml. The collected volume was measured by registering the water level using a ruler placed on the side of the bucket. The water levels were deduced from horizontal pictures, with an accuracy of ±0.25 mm. Hence, the volume measuring error was 4.45 ml, which is, for volumes measured in one minute, 0.20% of extreme flow, 0.40% of high flow, and 0.80% of low flow.

2.3. Materials

This study explores the hydraulic performance of two types of PPs: PA and PIP, two of the most used pavements [27]. Both were laid out over a base layer of small gravel (also named soil), with a geotextile below, laid over a subbase layer of big gravel (also named storage or STOR). Materials were first tested individually, and those layouts were named *PAind*, *PIPind*, *SOIL*, and *STOR70/140*. The individual layer analysis required additional materials, such as plastic cells (named cells), as a base for top layer materials, and a mosquito mesh (named mesh) to avoid material loss from PIPs. All layouts were placed over the waterproof membrane (named membrane), which provided flow parallel to the bench inclination. Complete layouts were named *PAcom* and *PIPcom*. All tested layouts and materials are given in Fig. 3. An image of the tested materials is also provided in Fig. 4

A local supplier, Asfaltia, laid the PA on top of an existing concrete surface and compacted it with a roller. Later, it was cut into square pieces of 0.50 m × 0.50 m to be joined together in the test bench. The joints between pieces were filled with standard silicone to avoid infiltration. PA was laid in two layers. The first layer, the one below and named PA16, was 5 cm thick, with a maximum aggregate size of 16 mm. The one above, PA11, was 4 cm thick, with a maximum aggregate size of 11 mm. The percent of binder by mass in the mixture was 4.3% for PA16 and 4.4% for PA11. The binder in both cases was polymer-modified bitumen, with a softening point of 70 °Celsius and penetration values at 25 °Celsius of 45/80, in 0.1 mm. The porosity was 20% (void ratio of 25%) for both layers. The hydraulic permeability was 250 000 mm/h for the complete section, measured using a constant head permeameter.

PIPs were AQUATA clay paving blocks from Wienerberger. PIP's dimensions were 80 mm thick, 200 mm long, and 63 mm wide. The PIPs had protrusions that left a void space between them and allowed water

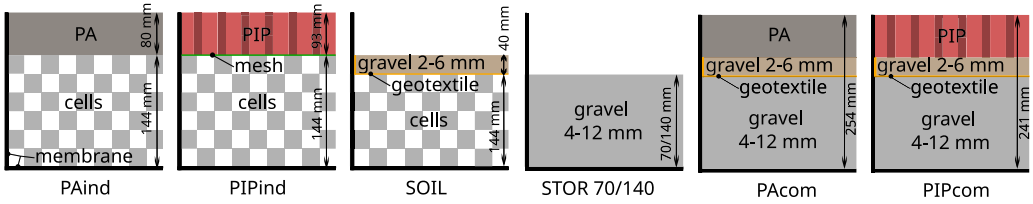

Fig. 3. Tested cross-sections, the first four for individual layers (PAind, PIPind, SOIL and STOR70/140), and the last two for complete layouts (PAcom and PIPcom).

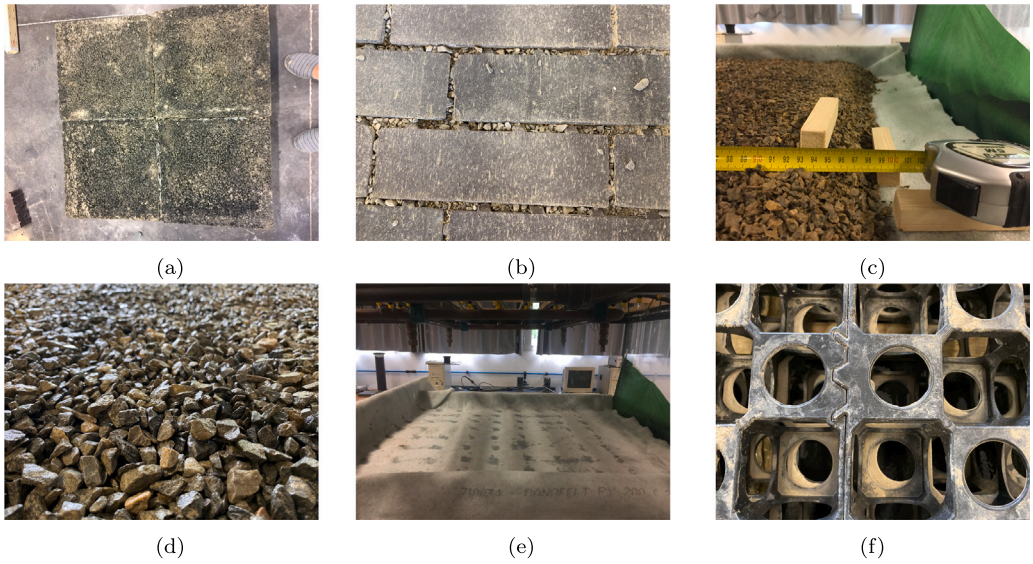

Fig. 4. Tested materials (a) PA, (b) PIPs with filled voids, (c) gravel 2/6 mm, (d) gravel 4/12 mm, (e) geotextile, and (f) plastic cells.

to infiltrate; those protrusions were 6 mm × 6 mm. Thus, the surface block had an empty volume of 9.84%, filled with the same small gravel used as a base material [5], described below. Considering the latter value and the void ratio of the filling material without being compacted, the PIP's void ratio was 0.05. The hydraulic permeability of PIPs was measured with the same permeameter used for PA, but the measured permeability was 90 000 mm/h.

The bedding or soil layer was 40 mm thick, formed with small limestone gravel, sizes between 2 and 6 mm. The gravel was compacted in the experimental bench after being laid. The porosity of the gravel was experimentally determined in a 100 ml plastic beaker, filling the pores with water and weighing additional water, replicating the measure three times. Measured mean values were 0.45 (void ratio of 0.82) for compacted gravel and 0.49 (void ratio of 0.97) for uncompacted one. Additionally, non-woven polyester geotextile, Danofelt PY 200 from Danosa, was placed below the bedding layer. The water permeability perpendicular to the unloaded plane for geotextile is at least 18 000 mm/h, according to the manufacturer specifications complying with UNE EN ISO 11058 standard.

Storage gravel was limestone gravel, with sizes between 4 mm and 12 mm [28]. The layer was tested with two thicknesses as an individual layer, 70 and 140 mm. Both thicknesses were selected considering depth limitations on the test bench. The first was the highest possible depth for the complete layout, and the second was selected considering the minimum recommended depth for pedestrian areas [28–30]. Those layers were named *STOR70* and *STOR140*. Gravel was compacted in place by hand. Void ratios were measured the same way as smaller gravel but using a 500 ml bucket instead. The measured porosities were equal to the ones obtained for the small gravel.

In addition to the examined material, plastic cells and a mosquito mesh were used in the individual layer configuration. The plastic cells, provided by Atlantis, were 52 mm thick and had a porosity of 90%. The cells were placed on cross-sections *PAind* and *PIPind*, as well as on the SOIL layout, as shown in Fig. 3. The mosquito mesh was located on the *PIPind* configuration, below the pavers, and above the plastic cells. The cells allowed fast water flow and minimised the influence on the outflow. The mesh prevented material loss from the PIP joints to the cell holes below.

2.4. Experimental procedure

The experimental procedure consisted of applying three precipitation regimes for 15 min to the selected cross-sections given in Fig. 3 under three defined slopes [28,31,32]: 1%, 2%, and 6%. Those three slopes are pavement and cross-section slopes simultaneously, as layout depth is constant. Under those configurations, outflow from the cross-sections was measured for 30 min. The experiments were replicated three times for each configuration. As each layout had nine configurations, a total of 189 hydrographs were measured.

The outflow was measured in the buckets at the circuit's end. In order to correctly capture the beginning and end of the hydrographs, considered time intervals were not constant. Thus, these are interval ending points: 1:00, 1:30, 2:00, 2:30, 3:00, 3:30, 4:00, 4:30, 5:00, 5:30, 6:00, 7:00, 8:00, 9:00, 11:00, 13:00, 15:00, 15:30, 16:00, 16:30, 17:00, 17:30, 18:00, 19:00, 20:00, 22:00, 25:00, and 30:00. Hence, the considered flows will be the average flow of those intervals, referred to mid-point of the interval. Consequently, measured hydrographs had 28 flow points. Previously calibrated rotameters were used to control inflow visually and set it to the theoretical *low/high/extreme* value. Applied real inflow in each experiment was calculated with the display value given by the flowmeter, which was, once placed on the test bench, also previously calibrated.

A standard systematic wetting process was designed for all experiments. The process involved a steady rain for 5 min followed by a dry interval of 5 min. After those initial 10 min, the principal experiment was conducted. The process has been graphically described in Fig. 5,

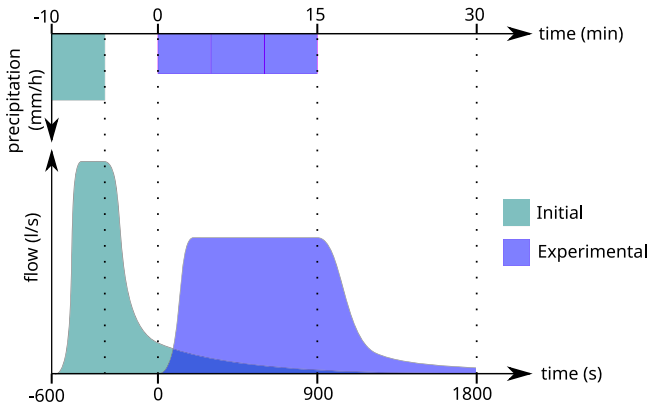

Fig. 5. A diagram with the experimental procedure, with analysed experimental precipitation/hydrograph in blue and initial wetting rain/hydrograph in green. (For interpretation of the references to colour in this figure legend, the reader is referred to the web version of this article.)

setting the beginning of the experimental hydrograph as the initial time.

The recession curve of the wetting process was first deduced to discriminate the effect of the initial wetting process on the experimental hydrograph [33], depicted as the overlapping hydrograph surfaces in Fig. 5. The exponential method was selected for that purpose [34], and Eq. (1) was used to define the recession curve, where Q_0 is the flow at the beginning of the recession curve, α is a constant related to section characteristics, and t is the time from the beginning of the recession curve. The higher the α, the faster the outflow from the section.

$$Q_t = Q_0 \cdot e^{-\alpha \cdot t} \tag{1}$$

The selected rain intensity for the wetting process was 140 mm/h, as it provided the highest flow value for the recession curve and, consequently, the lowest error, which increased with decreasing flows. Therefore, the recession curve of the wetting process was calculated based on linear regression with Eq. (1). Then, laboratory data were calculated as the difference between the measured hydrographs and wetting process hydrographs.

This procedure accepts that the grains are not completely dry initially. Given the number of planned tests and their duration, the time required to ensure a completely dry section would be unaffordable. On the contrary, the created wetting condition aims to ensure an equivalent initial condition for all tests. The wetting process's impact on the results will be discussed later.

2.5. Experimental hydrograph characterisation

Several parameters were calculated to characterise the hydraulic performance of studied cross sections, defined below [9,27]. The first two are typical parameters used to characterise the hydrologic performance of PPs. The late two provide additional information regarding retention capacity.

(a) Outflow Peak (OP), as the maximum outflow peak measured at the outlet;
(b) Time to Peak (TP), as the time elapsed from the beginning of rainfall to outflow peak;
(c) Timing Indexes (T_{50} and T_{80}), the time to a certain cumulative discharge, as percent, of inflow or precipitation.

2.6. Modelling data

This section will describe, firstly, (2.6.1) the model used to simulate the hydrographs obtained in the laboratory, (2.6.2) how that model has been set up to create artificial hydrographs, and, last, (2.6.3) selected criteria to analyse model performance and perform the calibration process. The methodology followed to simulate, calibrate and compare modelling data is summarised in Fig. 6.

2.6.1. Storm Water Management Model

SWMM is a dynamic rainfall-runoff simulation model used for a single event or long-term (continuous) simulation of runoff quantity and quality from primarily urban areas [35]. Since its origin, SWMM has implemented several SUDS, named LID controls in the model, the permeable pavement being one of them. PP is defined as a combination of several layers: Surface, Pavement, Soil, Storage, and Drain. Two of those layers are optional, Soil and Drain layer.

During the selected simulation time and applying the specified time steps, SWMM performs a moisture balance between layers. It keeps track of water transfers and determines how PP transforms inflow hydrographs into a runoff, sub-surface storage, sub-surface drainage, or infiltration into the native soil. Details about the used equations are given in [35]. In addition, [20,36] provide a more detailed description of the PP modelling process.

Defined PP may have two inflows, precipitation, and inflow from another area, which can be another subcatchment of another area from the subcatchment where PP is implemented. This study will just consider precipitation inflow. On the other hand, there may be three outflows from the layout: runoff, infiltration to native soil (seepage), or outflow from the drain. This study places the layout over an impermeable membrane, so infiltration to native soil will not be considered. Also, as initial tests confirmed, no runoff was created. Thus, the runoff will not be considered. Although evaporation is an outflow from the system, being a short-term analysis, it will not be considered either.

The PP can be implemented into a subcatchment, but there is another option, a subcatchment can be fully occupied by the LID control. For this study, a subcatchment fully occupied by PP has been considered. The 28 input parameters used by the model to perform the moisture balance are given in Table 1. As mentioned in the introduction, pavement clogging and drain control parameters were not considered.

2.6.2. Model setup

Six LID controls were defined in the model to simulate the hydrographs obtained in the laboratory, matching the ones shown in Fig. 3: four to check an individual layer and two with the complete cross-section. All LID controls were of the PP type. The parameters used to define each one are shown in Table 1.

The table parameters were given a known value when it was physically measured. When the values were not quantified, a calibration process was carried out, which will be detailed later. Those calibrated values are shown with the symbol * in the table. For calibration purposes, individual layers were used, and obtained values were applied to the complete cross-sections.

The LID controls had all a surface of 1 m^2 and were considered a subcatchment entirely occupied by a LID control of PP type. The outfall from the subcatchment was directed to a couple of nodes. The first one, *Runoff*, collected surface runoff, and the second one, *Drain*, collected outfall infiltrated from the permeable surface that percolated through the section. There are two additional nodes, *Junction* and *Outfall*, which were only created to provide an outlet for the water collected by the other two nodes. The *RainGauge* object provided the precipitation for the *PPsurface* subcatchment.

The selected time step for computing purposes was 1 s for both Wet Weather and Dry Weather. All the hydrograph values used to analyse the model performance were collected from the *Drain* element, where inflows to that element were stored. In order to compare experimental data with modelling data, gathered hydrographs were transformed into a 28-point hydrograph, with measuring points equal to that measured in the laboratory, and described in Section 2.4.

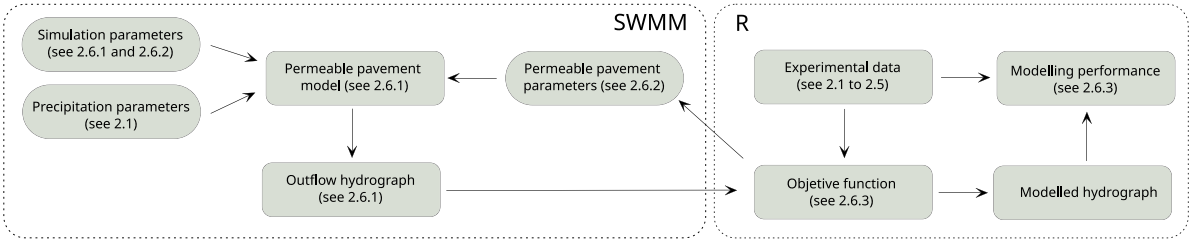

Fig. 6. Flowchart describing the methodology followed to obtain modelling results. On the left data managed with SWMM and, on the right, data managed with R.

Table 1
SWMM parameters for the PP type of LID control.

LAYER/Parameter	Units	Individual				COMPLETE	
		STOR70/140	Soil	PAind	PIPind	PAcom	PIPcom
Surface							
Berm height, D_1	mm	0	0	0	0	0	0
Veget. Vol. Frac., $1-\phi_1$	–	0	0	0	0	0	0
Roughness, n	s $m^{-1/3}$	0.02	0.02	0.017[a]	0.016[a]	0.017	0.016
Slope, S	%	1-2-6	1-2-6	1-2-6	1-2-6	1-2-6	1-2-6
Pavement							
Thickness, D_4	mm	0.01	0.01	93	80	93	80
Void ratio, $\phi_4/(1-\phi_4)$	Voids/Solids	0.99	0.99	0.25	0.97	0.25	0.97
Imperv. Surf. Frac., F_4	–	0	0	0	0.9	0	0.9
Permeability, K_4	mm/h	100 000	100 000	250 000	90 000	250 000	90 000
Clogging factor, –	–	0	0	0	0	0	0
Regen. interval, –	days	0	0	0	0	0	0
Regen. fraction, –	–	0	0	0	0	0	0
Soil							
Thickness, D_2	mm	0	38	0	0	0	0
Porosity, ϕ_2	vol. frac.	–	0.44	–	–	–	–
Field capacity, θ_{fc}	vol. frac.	–	0.09[a]	–	–	–	–
Wilting point, θ_{wp}	vol. frac.	–	0.03	–	–	–	–
Conductivity, K_{2S}	mm/h	–	100 000[a]	–	–	–	–
Cond. slope, HCO	–	–	40	–	–	–	–
Suction head, ψ_2	mm	–	80	–	–	–	–
Storage							
Thickness, D_3	mm	77–159	144	144	144	85	85
Void ratio, $\phi_3/(1-\phi_3)$	Voids/Solids	0.82	0.99	0.99	0.99	0.82	0.82
Seepage rate, K_{3S}	mm/h	0	0	0	0	0	0
Clogging factor, –	–	0	0	0	0	0	0
Drain							
Flow coefficient, C_{3D}	–	8[a]–7[a]	600[a]	18[a]	4[a]	7.5	7.5
Flow exponent, K_{3D}	–	1.6[a]–1.6[a]	0.2[a]	1.6[a]	1.5[a]	1.6	1.6
Offset, D_{3D}	mm	0	0	0	0	0	0
Open level, –	mm	–	–	–	–	–	–
Closed level, –	mm	–	–	–	–	–	–
Control curve, –	–	–	–	–	–	–	–

[a]Values obtained after calibration process.

2.6.3. Model performance and calibration

The Nash–Sutcliffe adimensional coefficient (NSE) was selected to compare modelled hydrographs with experimental ones [37]. The NSE values are given in Eq. (2), where O_i and $\overline{O}_i$ are experimental values and M_i are modelled ones. NSE values range from $-\infty$ to 1, where a value equal to 1 indicates a perfect fit.

$$NSE = 1 - \frac{\sum_{i=1}^{N}(O_i - M_i)^2}{\sum_{i=1}^{N}(O_i - \overline{O}_i)^2} \quad (2)$$

As part of the model parameters were physically measured, individual cross sections were considered a source for unmeasured data (see Table 1). A calibration process was carried out to set those unmeasured parameters. Once individual layer calibration was conducted, those values were introduced in the complete cross-sections to check the model performance.

However, as the soil layer had several unmeasured parameters which should be calibrated, just conductivity and field capacity were allowed to vary during calibration. The remaining unmeasured soil parameters, wilting point, conductivity slope, and suction head, were fixed to a value obtained from the SWMM manual based on a previously conducted sensitivity analysis [20]. Considered parameter ranges for the calibration process are given in Table 2.

Table 2
Maximum, minimum and initial parameter values for calibration purposes.

Parameter	Units	Minimum	Maximum	Initial value
Roughness (n)	s $m^{-1/3}$	0.01	0.02	0.015
Field capacity (θ_{fc})	vol. frac.	0.06	0.2	0.1
Conductivity (K_{2S})	mm/h	0	100 000	500
Flow coefficient (C_{3D})	–	0	1000	5
Flow exponent (K_{3D})	–	0	100	1

Differential Evolution Algorithm (DEA) was used for calibration purposes, which is particularly convenient for finding the global

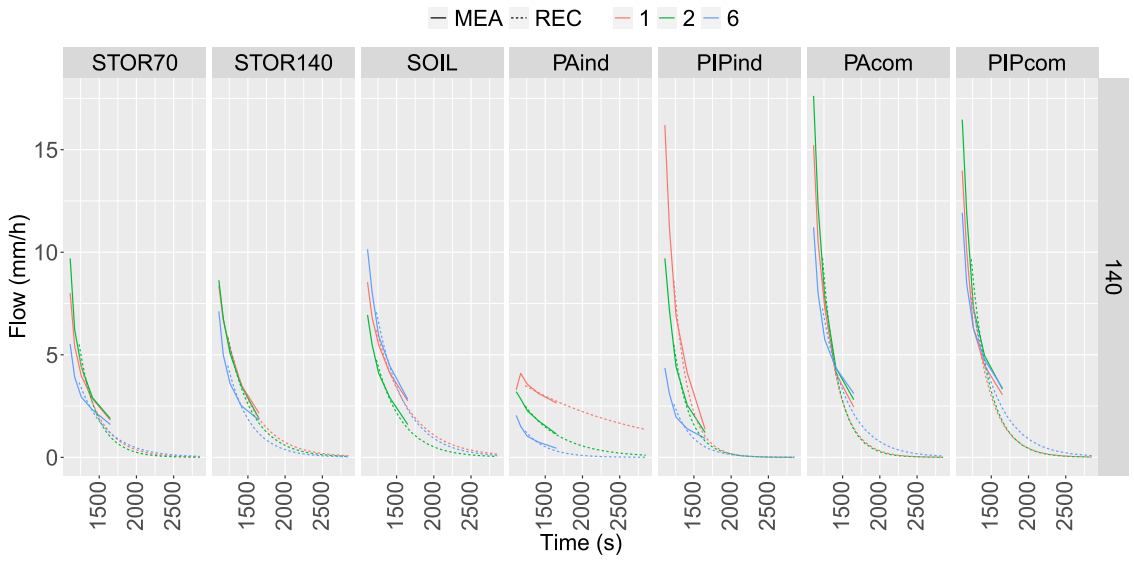

Fig. 7. Recession curve baselines (continuous line, named MEA) and extrapolated ones (dotted lines, named REC) for 140 rain, different colours are shown for each slope.

optimum of a real-valued function of a real-valued parameter and not requiring a continuous or differentiable function [38]. Calibrated values were obtained with the differential evolution algorithm provided by the *DEoptim* package for the *R* programming language [39]. The selected objective function for calibration purposes was previously defined in Eq. (2). Calibration for all hydrographs of the same layout was conducted once. Thus, the objective function was $\sum_{i=1}^{i=9} NSE_i$.

In order to compare modelled results with laboratory tests, both Peak and Volume errors were also analysed [40], named *Pe* and *Ve*:

$$error \quad (\%) = \frac{X_{model} - X_{experimental}}{X_{experimental}} \cdot 100 \tag{3}$$

3. Results

To provide an analysis of the experimental hydrographs and compare them with the ones provided by the model, experimental hydrographs are presented first (Section 3.1), and model performance later (Section 3.2).

3.1. Experimental data

No runoff was observed at any experimental setup or layout. Nevertheless, slight water losses were observed due to raindrop splashes, which went out of the bench after contacting the surface. This phenomenon has mainly been observed with PIPs.

3.1.1. Recession curve

Calculated recession curves were 21, all for the 140 mm/h rainfall used in the initial wetting process, one for each cross-section and slope. Measured curve (MEA), used as a baseline, and extrapolated recession curves (REC), using Eq. (1), are given in Fig. 7. Note that the time axis starts at 1200 s in that Figure, as explained by the procedure detailed in Fig. 5. Data shows that, generally, the recession curve tends to be lower than measured at the beginning of the extrapolation.

Outflow hydrographs (laboratory or LAB) were calculated based on deduced curves, detracting recession values (REC) from measured ones (MEA). Deduced LAB curves, to be used from now on, together with measured and recession curves, are shown in Fig. 8. Only hydrographs related to PAcom layout are shown to simplify the image. Initial flow values are close to zero in all cases.

3.1.2. Laboratory hydrographs

Regarding laboratory hydrographs, the ones being analysed hereafter, Fig. 9 shows differences between layouts. Only PIP-related hydrographs were plotted in this case. Visual analysis shows that the peak is reached earlier for thinner layers. It also can be noticed that the storage layer reaches the peak slower than the other two single layers, soil and PIPind. In addition, the delay of the peak results in higher outflows during the last half of the experiment.

Fig. 10 is provided for detailed peak analysis, showing all considered cases. Higher rain intensities create higher peaks. Also, thicker layouts create higher peaks, in general. It is not the case for the soil layer, which shows similar peaks in the thinnest storage layer. Although higher slopes provide greater peaks as a general rule, there are some cases where the highest peak does not correspond to the highest slope. On the surface layer, results also show a higher peak for PIPind than for PAind.

Detailed time-to-peak values are given in Fig. 11. It can be observed that the thicker the section, the higher the time to the peak. However, PAind indices are clearly lower than soil ones. Also, higher rains result in faster peaks. For complete layouts and small rains, the maximum peaks are around 900 s, close to the end of the rainfall. It also can be noted that higher slopes yield a lower time to peak, in general, although complete layouts do not follow that pattern.

Concerning the time indices obtained, given in Fig. 12, lower precipitation intensities result in higher time indices. On the contrary, the slope influence on time indexes needs to be clarified. The case with a different pattern is the soil layer, where 6% time indexes are higher than 2%. A thicker section yields a higher time index for analysed cross-sections, but some exceptions exist. PAind and PIPind are superficial layers, but both time indices differ, as PIPind shows higher indices than PAind. Also, although the soil layer is the thinnest, its time indices are higher than PIPind or PAind, even higher than the STOR140 layout for low rains.

3.2. Model performance

Individual layers are presented separately, as their hydrographs were used to calibrate unmeasured parameters from the model. Hence, complete layouts will be presented later using calibrated parameters obtained in the first section.

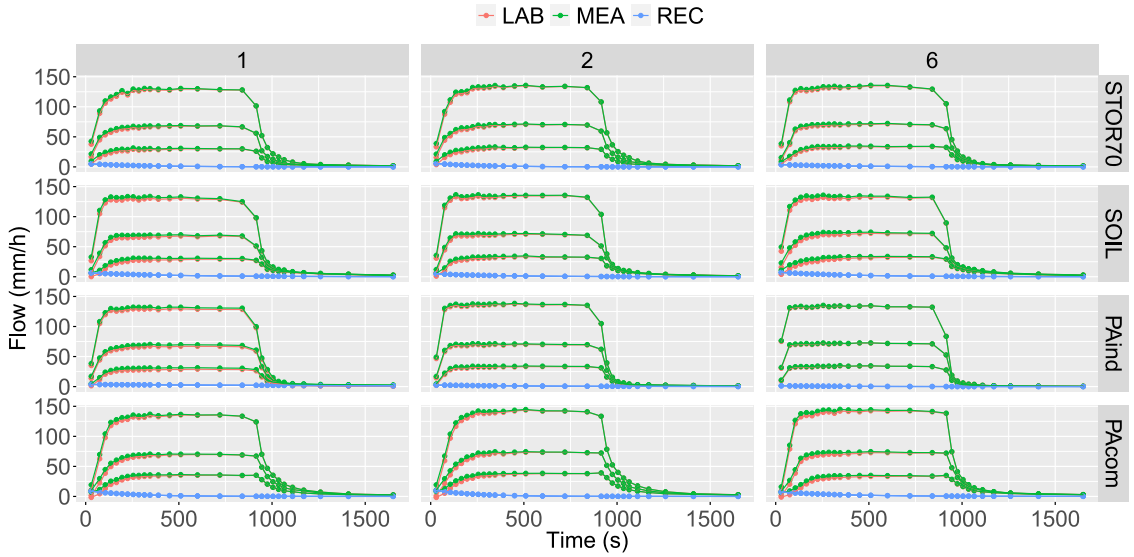

Fig. 8. Measured hydrographs (green), recession curves (blue), and laboratory hydrographs (red) deduced from the first two. Only PA related layouts are shown, separated for different slopes (columns) and layouts (rows).

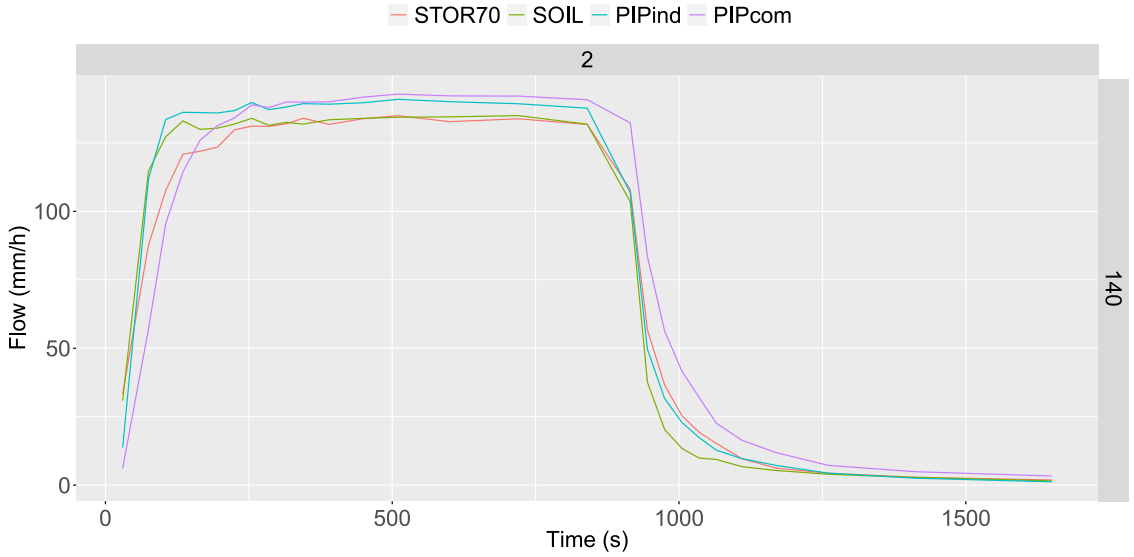

Fig. 9. Outflow from PIP related layouts for 140 rain and 2% slope, with different colours for each layout.

Table 3
NSE values for a layer-by-layer calibration.

Layer	STOR70/140	Soil	PAind	PIPind
Minimum NSE	0.832	−2.130	0.845	0.867
Average NSE	0.968	−0.851	0.959	0.954
Maximum NSE	0.993	0.153	0.991	0.988

3.2.1. Hydrographs by layer

The parameter values obtained from individual layer hydrographs after calibration are given in Table 1, together with the physically measured parameter values used during calibration. The NSE values corresponding to the calibration process are given in Table 3. Analysed by layer, the soil layer values are notably worse than other individual layers.

3.2.2. Hydrographs for complete layouts

Complete hydrographs were calculated using the parameter values calibrated in the previous section (see Table 1). The hydrographs were calculated without considering any soil layer in the model, as individual layer results showed an unsatisfactory output. NSE results comparing laboratory and modelled hydrographs are given in Fig. 13. The minimum value is 0.74, which can be considered good. PAcom yields slightly better results than the PIPcom layout.

Calculated Peak and Volume errors for modelled hydrographs are given in Fig. 14. Almost all errors are positive; thus, modelled hydrographs overestimate the volume and peak. Errors are higher for lower slopes. Average Pe and Ve are 3.2% and 2.8%. Both maximums are smaller than 8%, and both minimums are close to 0%.

4. Discussion

4.1. Experimental data

The lack of runoff is consistent with other laboratory studies for PPs [27] but is also in line with previous site experiments performed with PP systems [7,41,42]. This shows how effectively the new PP reduces runoff, especially for short individual events.

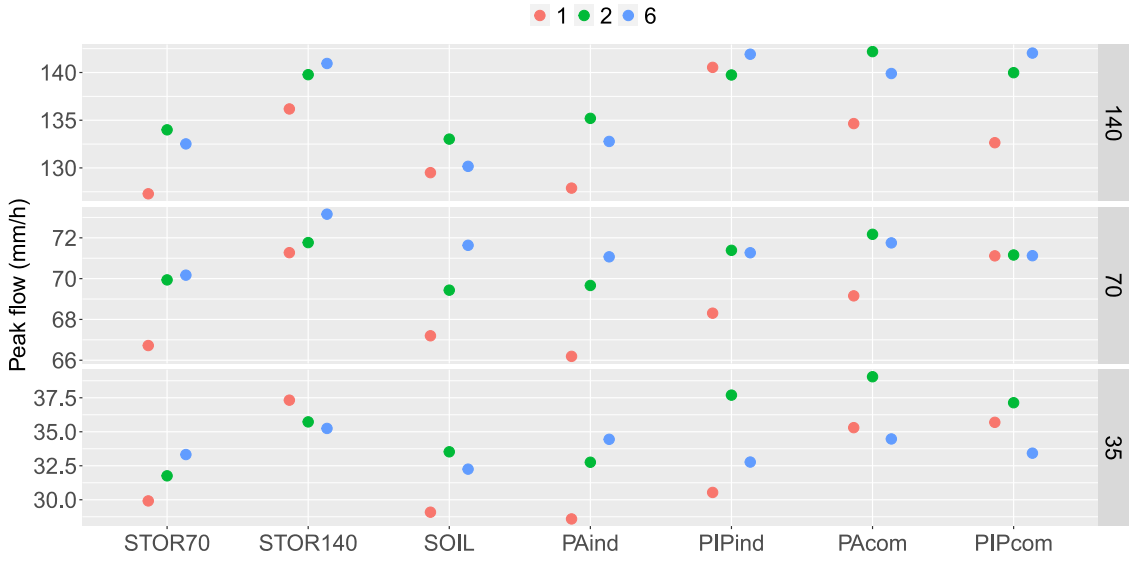

Fig. 10. Peak values from experimental cross-sections. Different colours and shapes are given for rain and slope cases.

Fig. 11. Time to peak values from experimental cross-sections. Different colours and shapes are given for rain and slope cases.

Higher raindrop splashes on PIPs are due to their horizontal surface. As PA and gravel provide irregular surfaces, they tend to split the raindrop, and the observed water loss was minimal. This phenomenon shall directly affect the level of comfort perceived by users if PIPs and PA are compared. In any case, losses have been considered negligible compared to measured water flows and volumes.

4.1.1. Recession curve

The visual analysis of Fig. 7 clearly shows that extrapolation considers lower flow rates than measured data in most cases. Nevertheless, obtained values were considered acceptable for calculating the impact of the initial wetting process during the last 1200 s of the experiment, as those recession flows were considerably lower than measured flows.

Although constant rain was applied during the experiment, and a constant outflow may be expected, a slightly decreasing flow tendency was noticed once the peak value was reached. However, that decreasing tendency was corrected after the recession curve values were detracted from measured ones. In particular, the obtained initial flow values were close to zero once recession values were detracted, showing that the flow measured during the first minute for those cases was mainly due to the initial wetting process. It also shows that the impact of the wetting process on the outflow was minimal.

4.1.2. Laboratory hydrographs

The first visual analysis from Fig. 9 may be considered consistent, as increasing layer thickness increases water retention. In that case, the time to peak and outflow are higher once the rain has stopped, which makes sense from a water balance perspective.

According to peak values shown in Fig. 10, higher slopes provide greater peaks than lower ones because the detention process is less significant in steeper slopes, as water is easier drained by gravity. Regarding the impact of depth, showing greater peaks for thicker layers differ from what initially may be expected. This effect is noticeable for two storage layers with different depths (STOR70 and STOR140). It may be expected that thicker layers delay outflow and reduce peak flow. An explanation may be that water can travel a longer path for thicker layers and, hence, more interstitial particle surface contributes to the outflow. Therefore, the peak is delayed but with a higher value. In addition, depths are not high enough to delay the beginning of the peak over rain duration, which contributes to the mentioned behaviour.

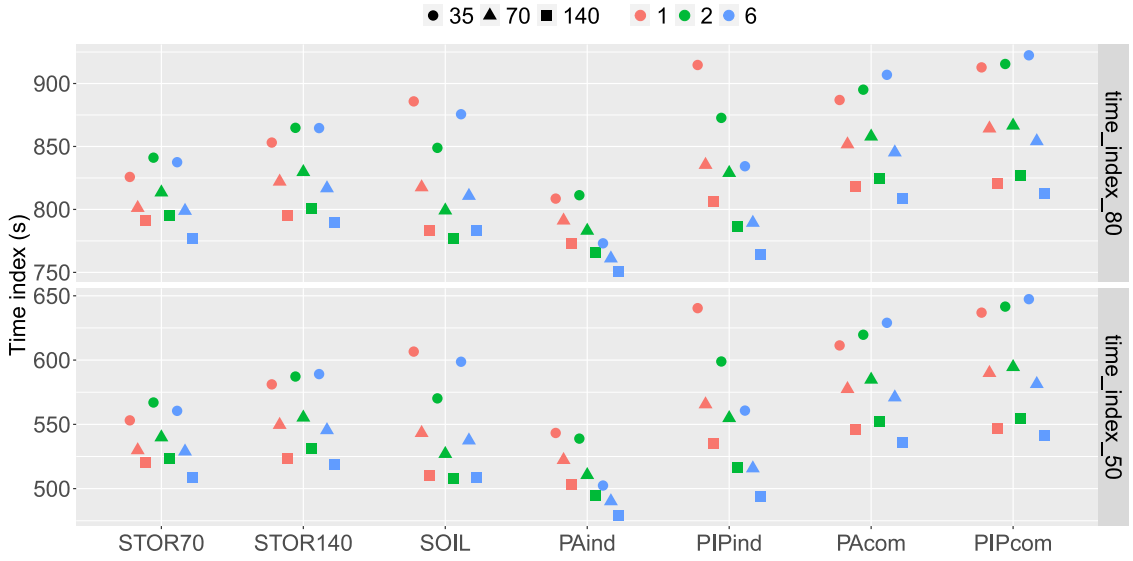

Fig. 12. Calculated time index values, T_{50} and T_{80}, for outflow hydrographs on experimental cross-sections. Different shapes are given for rain cases and different colours for slope cases.

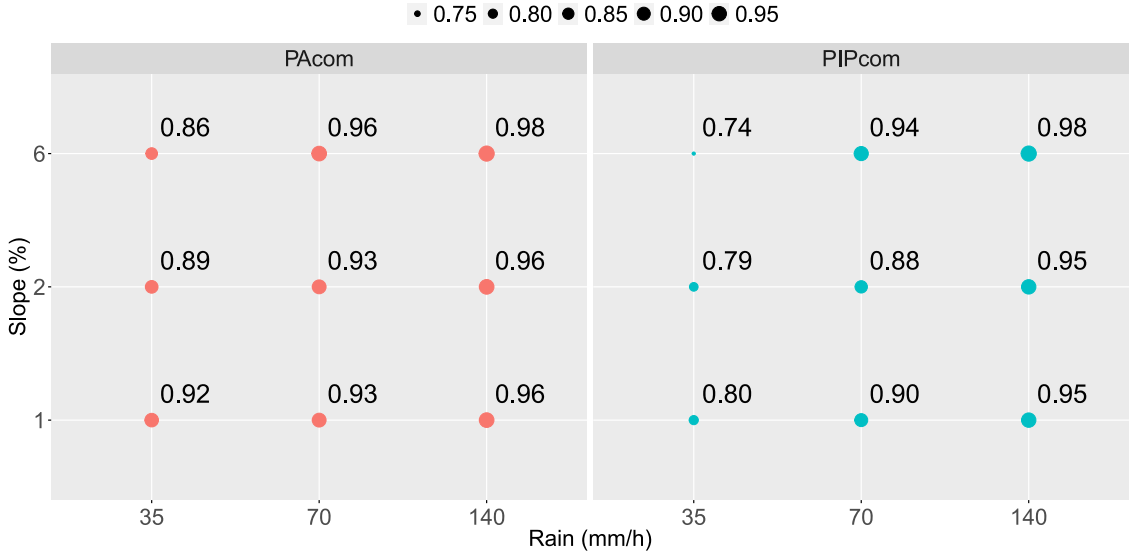

Fig. 13. Obtained NSE values given as point size for complete layouts, PAcom (red) and PIPcom (blue), with separated values for different rain and slope combination.

If time to peak is analysed, see Fig. 11, thicker cross-sections yield higher times to the peak, as may be expected. Thus, more time is needed for water to flow through the entire layout. However, individual superficial layers and individual storage layers respond differently. As storage layers are on the bottom, water flow is parallel to it and travels through the gravel section horizontally. Therefore, water needs more time to reach the exit; that is, the time to peak is greater. As complete layers also have the gravel layer beneath, they perform similarly. On the contrary, water flows freely over the membrane for superficial layers tested individually. Regarding the impact of rain intensity, higher rains result in faster peaks, probably because the section saturates faster and, thus, drains water out of the layout faster.

For complete layouts and small rains, the maximum peaks are around 900 s, close to the end of the rainfall, suggesting that the layout may still reach saturation. However, plotted hydrographs, such as the ones in Fig. 9, show that hydrograph slopes tend to be horizontal around 900 s, confirming layout has almost saturated completely.

About the time indices given in Fig. 12, it is clear that higher time indices for lower precipitation intensities suggest that the retention capacity of the pavement decreases as precipitation increases, as higher intensities indicate a higher precipitation volume. Concerning the slope influence on time indices, one might initially assume that the higher the slope, the lower the time index, as water is drained faster and the detention capacity of the section is reduced. That pattern is apparent for superficial PAind and PIPind layers. However, there is a discrepancy with the 1% slope in many other cases, as the time index is lower than that for higher slopes. That is the case for storage layers and most of the complete section values. A possible explanation for the soil layer behaviour, with a different pattern, may rely on the geotextile. The horizontal permeability of the geotextile may be altered for sloping positions. Also, a capillary barrier effect could affect differently for different section slopes to the vertical permeability of the geotextile.

In superficial layers, PIPind shows higher indexes than PAind, which the porosity-related properties of the sections may explain. Regarding the porosity distribution, PA has a uniform porosity, facilitating water infiltration as it reaches the surface. On the contrary, water over PIPs has to reach joints to infiltrate. On the other hand, PA's overall

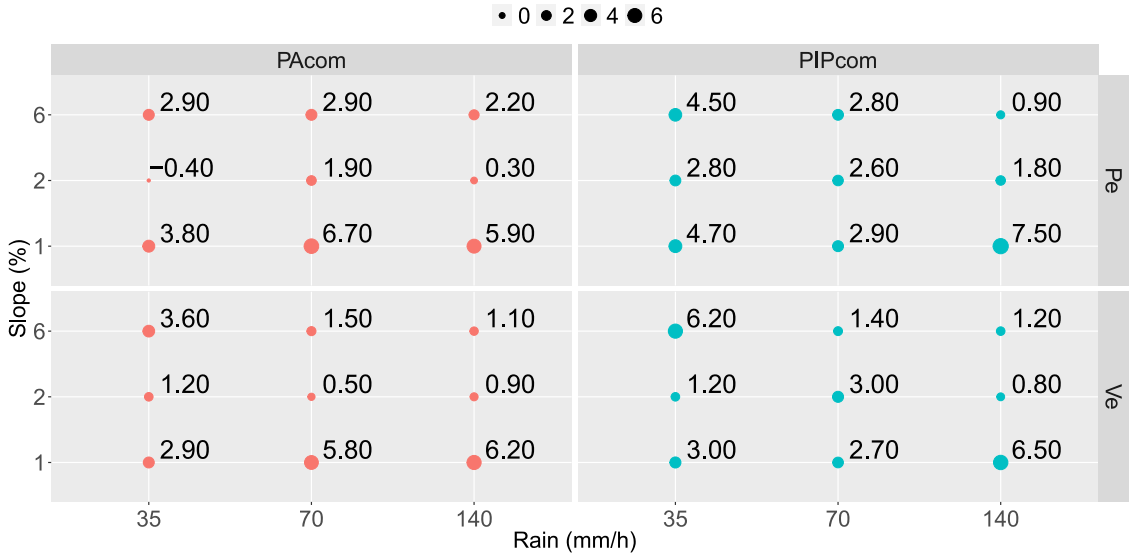

Fig. 14. Peak (Pe) and Volume (Ve) error for modelled hydrographs with complete layouts, PAcom (left) and PIPcom (right), size is proportional to error value.

porosity is higher than the porosity of the PIP. These two porosity-related characteristics may well explain the difference. Also, although the soil layer is the thinnest, its time indices are higher than PIPind or PAind, even higher than the 140 mm storage layer for low rains. This discordance may be due to the geotextile layer below the soil, which may influence the detention capacity of all the layers. In any case, the retention capacity performance is opposed to that found by Støvring et al. [7].

It should be noted that the experimental procedure may reduce the peak time compared to a dry layout, as first water does not adhere to material grains. The procedure may also reduce obtained time indexes compared to a completely dry section. Nevertheless, the procedure should not impact the peak value reached after the section is saturated. The values obtained here may be valid, as natural sections may often be wet in an Atlantic climate where rain is 180 days per year.

4.2. Model performance

4.2.1. Hydrographs by layer

Overall, average NSE values for individual layers show, see Table 3, that the model gives a very good response if physical parameters of the pavement are introduced and some unmeasured parameters are calibrated. Those unmeasured parameters were drain coefficient, exponent, and Manning n for pavements. This last parameter value obtained by calibration was close to those given by bibliographic references. On the contrary, drain parameters could not be obtained from bibliographic sources, as they have no physical meaning.

Except for the soil layer, the minimum NSE value is over 0.80, which can be considered a good prediction. However, the soil layer values are significantly poorer. For this layer, both experimental and modelled hydrographs are given in Fig. 15. It can be appreciated that it is difficult to capture the experimental hydrograph's initial flow for all analysed slopes and rain intensities. The model cannot reproduce initial outflow, although the performance improves for higher rain intensities.

The above may be related to the fact that the soil layer was conceived as engineered for bio-retention cells, where infiltration from the upper pavement layer is modelled based on the Green-Ampt equation [35]. As open-graded aggregates tend to drain more water by gravity than soils with smaller particles [7], this approach is not the most suitable for modelling gravel-type layers, even with a geotextile beneath. In that sense, the soil layer may be expected to represent the geotextile effect on the flow, but the results show the opposite.

4.2.2. Hydrographs for complete layouts

All modelled hydrographs showed good agreement, with an average NSE of 0.907, higher for PAcom (0.931) than for PIPcom (0.882). However, PIPcom under 35 rain and 6% slope present a minimum value of 0.74. All hydrographs are given in Fig. 16. The average value is higher than the one obtained by Platz et al. [16] after calibrating and validating on-site data; the average NSE was 0.74. Hydrographs predicted by a single controlled event may be expected to fit better with measured ones and get better predictions. However, Platz et al. [16] calibrated all parameters, and this study did not.

Overall, the model predicts a higher flow than the measured one. That discrepancy is more significant at the hydrographs' beginning and end, although it can also be observed at the peak values. The difference is higher for lower rain intensities and low slopes. That difference causes an advance in drained volume. It seems related to the drain coefficient and exponent used for modelling. As those two parameters do not have an actual physical meaning in the experiment, calibrated parameters for a single storage layer were used. Hence, as the single-layer outflow is faster than the complete-layer outflow (see Fig. 9), drain parameters advance outflow for the complete layout, which may be reduced if those two parameters were calibrated for a complete layout.

However, modelled hydrographs also show a flow value during the first measured minute, while laboratory hydrographs have almost no flow during the first minute. A faster experimental outflow may be expected due to the initial wetting process, but the results show the contrary. That model behaviour probably does not consider the initial water that covers material grains, delaying initial flow. Moreover, the first initial wetting process may forward experimental flow.

Modelling hydrographs overestimating experimental ones, given in Fig. 14, is probably related to the two reasons mentioned above, higher drain coefficient and exponent, and a faster flow, leading to overestimating the volume and the peak. However, errors may be considered reasonably low.

4.3. Research limitations and uncertainty

Although the authors consider that the results here presented are interesting and potentially useful for practitioners involved in the hydrologic design of PPs, the methodology proposed in this research presents certain limitations to be considered related to (a) the test bench dimensions, which are much smaller than real applications; (b)

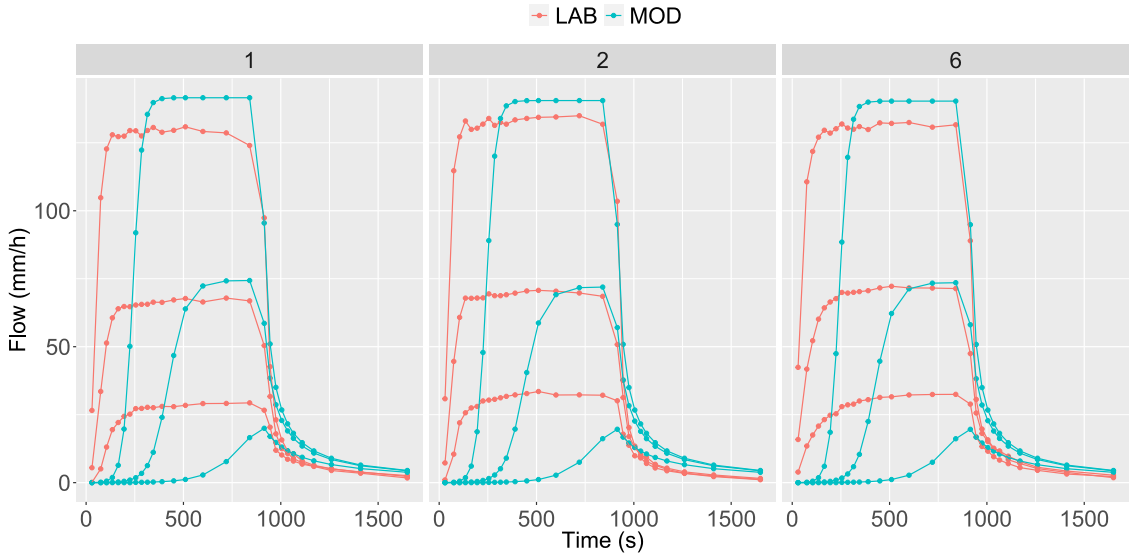

Fig. 15. Experimentally measured hydrographs (red) and modelled ones (blue) for individual soil layer. Different slopes are given in columns. Average NSE is −0.851. (For interpretation of the references to colour in this figure legend, the reader is referred to the web version of this article.)

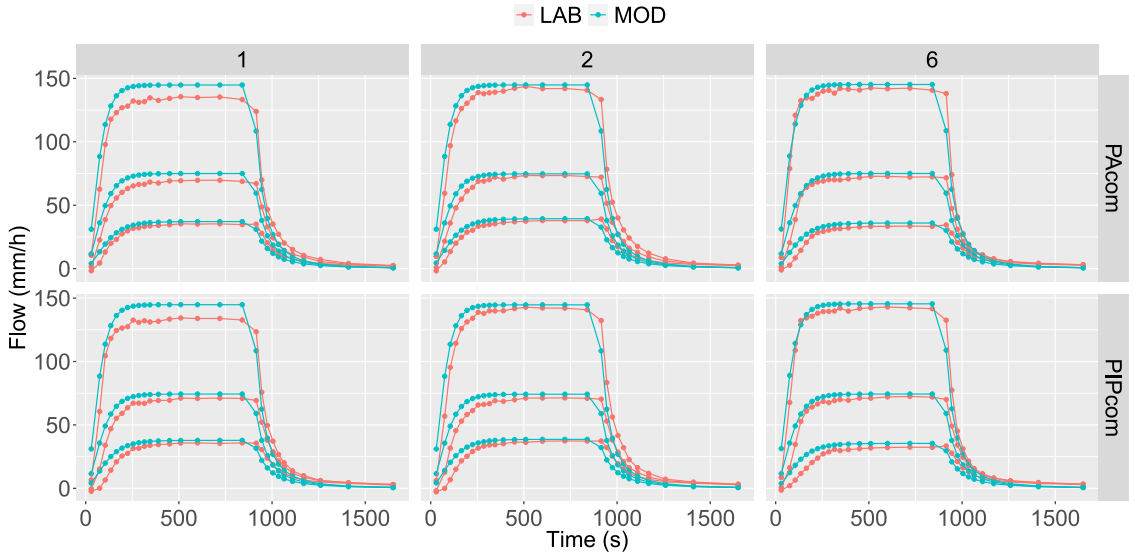

Fig. 16. Experimental (red) and modelled (blue) hydrographs for complete layouts. Different sections are given in rows and slopes in columns. (For interpretation of the references to colour in this figure legend, the reader is referred to the web version of this article.)

the materials selected for the surface, which are limited to new unclogged pavements; (c) the material selected for the base layer; (d) the methodological aspect, such as applied uniform rain or selected wetting process; (e) the systematic errors generated during the measurement process, as flow starting/stopping time; (f) the human errors made during the experimental process; and, (g) the assumptions made during the research process, such as neglecting water losses that took place during experiments.

5. Conclusion

The main contribution of this study is to explore the deficiencies of a highly used conceptual model by detailing how each of the individual layers contributes to the complete layout performance, which is a novel contribution to the literature. Based on layer-by-layer experimental data, the research first analysed how rain intensity and slope influenced the outflow from two types of permeable pavements: PIPs and PA. Later, it analyses the hydrological performance of those pavements when modelled with one of the most popular urban drainage models, the Storm Water Management Model.

Experimental results confirm, in line with previous studies, that PP systems are an excellent option to delay runoff response in urban environments, as they provide a higher detention capacity than traditional pavements. Results also reveal that the detention capacity of the superficial PIPind layer is notably higher than that provided by PAind, which is probably related to its pore distribution, although peak values are higher for the PIPind layer. Also, it was found that detention capacity increases for low rain volumes and lower slopes. However, the influence of a sloping geotextile remains uncertain, and further research is recommended.

On the other hand, modelling results show that the model performance is generally quite good without considering the base and subbase layers as one, with a geotextile between them. However, the model forwards the flow if compared to the experimental one. Besides, drain outflow modelling based on orifice parameters makes it difficult to set drainage coefficient and exponent for cases that do not match

mentioned physical orifice-type drains. The latter induces a faster initial outflow for modelled hydrographs. The study also found that calibrated Manning values were close to those given by bibliographic references. In any case, further study of the drainage outflow model is advisable to understand how its parameters can condition the outflow. It also would be interesting to deepen the study of long-term performance under laboratory conditions.

Another interesting finding in the modelling part relates to the optional soil layer given in the model. That layer definition was not valid for gravel-type base layers. Its hydraulic behaviour does not match a soil-type layer defined using the Green-Ampt equation, even with a geotextile below. Thus, those layers, including the geotextile, shall be modelled along with the storage layer. For a better understanding of the model, it would be interesting to study how sandy soils may perform, on the one hand, and how the geotextile layer may be modelled in order to capture its hydraulic properties better.

In summary, the two main contributions of this article are to explain in detail the performance of each layer contained in a PP system and the validation of modelling results for the complete layout without calibration. The first one shall be useful for researchers and practitioners to understand each layer's influence better, both for design and modelling purposes. The second one shall increment designers' confidence in the modelling results when the complete layout cannot be calibrated. In short, the results obtained in this study are expected to increase practitioners' confidence while integrating a PP model into an urban subcatchment based on physical parameters that can be easily measured or predicted, but also where it is unfeasible to calibrate the PP model.

CRediT authorship contribution statement

Eneko Madrazo-Uribeetxebarria: Conceptualization, Data curation, Formal analysis, Investigation, Methodology, Resources, Software, Visualization, Writing – original draft. **Maddi Garmendia Antín:** Funding acquisition, Project administration, Supervision, Writing – review & editing. **Gorka Alberro Eguilegor:** Investigation. **Ignacio Andrés-Doménech:** Formal analysis, Supervision, Validation, Writing – review & editing.

Declaration of competing interest

The authors declare that they have no known competing financial interests or personal relationships that could have appeared to influence the work reported in this paper.

Data availability

Data will be made available on request.

Acknowledgements

This research was funded by the University of the Basque Country UPV/EHU grant number US22/10. It was also supported by Donostia/San Sebastián City Council, to which we are very grateful for providing us with the material for the experimental part.

References

[1] S. Charlesworth, R. Wade, Multiple benefits from surface water management – SUDS, Clean – Soil Air Water 42 (2) (2014) 109–110, http://dx.doi.org/10.1002/clen.201470014.

[2] T.D. Fletcher, W. Shuster, W.F. Hunt, R. Ashley, D. Butler, S. Arthur, S. Trowsdale, S. Barraud, A. Semadeni-Davies, J.L. Bertrand-Krajewski, P.S. Mikkelsen, G. Rivard, M. Uhl, D. Dagenais, M. Viklander, SUDS, LID, BMPs, WSUD and more – The evolution and application of terminology surrounding urban drainage, Urban Water J. 12 (7) (2015) 525–542, http://dx.doi.org/10.1080/1573062X.2014.916314.

[3] U. Kuruppu, A. Rahman, M.A. Rahman, Permeable pavement as a stormwater best management practice: a review and discussion, Environ. Earth Sci. 78 (10) (2019) http://dx.doi.org/10.1007/s12665-019-8312-2.

[4] N. Xie, M. Akin, X. Shi, Permeable concrete pavements: A review of environmental benefits and durability, J. Clean. Prod. 210 (2019) 1605–1621, http://dx.doi.org/10.1016/j.jclepro.2018.11.134.

[5] J. Mullaney, T. Lucke, Practical review of pervious pavement designs, Clean - Soil Air Water 42 (2) (2014) 111–124, http://dx.doi.org/10.1002/clen.201300118.

[6] N. Tziampou, S.J. Coupe, L.A. Sañudo-Fontaneda, A.P. Newman, D. Castro-Fresno, Fluid transport within permeable pavement systems: A review of evaporation processes, moisture loss measurement and the current state of knowledge, Constr. Build. Mater. 243 (2020) 118179, http://dx.doi.org/10.1016/j.conbuildmat.2020.118179.

[7] J. Støvring, T. Dam, M.B. Jensen, J. Stovring, T. Dam, M.B. Jensen, Hydraulic performance of lined permeable pavement systems in the built environment, Water 10 (5) (2018) http://dx.doi.org/10.3390/w10050587.

[8] L.A. Sañudo-Fontaneda, J. Rodriguez-Hernandez, A. Vega-Zamanillo, D. Castro-Fresno, Laboratory analysis of the infiltration capacity of interlocking concrete block pavements in car parks, Water Sci. Technol. 67 (3) (2013) 675–681, http://dx.doi.org/10.2166/wst.2012.614.

[9] J. Rodriguez-Hernandez, V.C. Andrés-Valeri, A. Ascorbe-Salcedo, D. Castro-Fresno, Laboratory study on the stormwater retention and runoff attenuation capacity of four permeable pavements, J. Environ. Eng. 142 (2) (2016) 04015068, http://dx.doi.org/10.1061/(ASCE)EE.1943-7870.0001033.

[10] M. Kamali, M. Delkash, M. Tajrishy, Evaluation of permeable pavement responses to urban surface runoff, J. Environ. Manag. 187 (2017) 43–53, http://dx.doi.org/10.1016/j.jenvman.2016.11.027.

[11] M. Alsubih, S. Arthur, G. Wright, D. Allen, Experimental study on the hydrological performance of a permeable pavement, Urban Water J. 14 (4) (2017) 427–434, http://dx.doi.org/10.1080/1573062X.2016.1176221.

[12] C.Y. Liu, T.F.M. Chui, Factors influencing stormwater mitigation in permeable pavement, Water 9 (12) (2017) 988, http://dx.doi.org/10.3390/w9120988.

[13] C. Xu, T. Tang, H. Jia, M. Xu, T. Xu, Z. Liu, Y. Long, R. Zhang, Benefits of coupled green and grey infrastructure systems: Evidence based on analytic hierarchy process and life cycle costing, Resour. Conserv. Recy. 151 (April) (2019) 1–10, http://dx.doi.org/10.1016/j.resconrec.2019.104478.

[14] K. Eckart, Z. McPhee, T. Bolisetti, Performance and implementation of low impact development - A review, Sci. Total Environ. 607 (2017) 413–432, http://dx.doi.org/10.1016/j.scitotenv.2017.06.254.

[15] S. Kaykhosravi, U.T. Khan, A. Jadidi, A comprehensive review of low impact development models for research, conceptual, preliminary and detailed design applications, Water 10 (11) (2018) http://dx.doi.org/10.3390/w10111541.

[16] M. Platz, M. Simon, M. Tryby, Testing of the storm water management model low impact development modules, J. Am. Water Resour. Assoc. 56 (20) (2020) 283–296, http://dx.doi.org/10.1111/1752-1688.12832.

[17] S. Zhang, Y. Guo, SWMM simulation of the storm water volume control performance of permeable pavement systems, J. Hydrol. Eng. 20 (8) (2015) 06014010, http://dx.doi.org/10.1061/(ASCE)HE.1943-5584.0001092.

[18] M. Randall, J. Støvring, M. Henrichs, M. Bergen Jensen, Comparison of SWMM evaporation and discharge to in-field observations from lined permeable pavements, Urban Water J. (2020) 1–12, http://dx.doi.org/10.1080/1573062X.2020.1776737.

[19] E. Madrazo-Uribeetxebarria, M. Garmendia Antín, J. Almandoz Berrondo, I. Andrés-Doménech, Hydraulic performance of permeable asphalt and PICP in SWMM, validated by laboratory data, in: WIT Transactions on Ecology and the Environment, Vol. 238, WitPress, 2019, pp. 569–579, http://dx.doi.org/10.2495/SC190491.

[20] E. Madrazo-Uribeetxebarria, M. Garmendia Antín, J. Almandoz Berrondo, I. Andrés-Doménech, Sensitivity analysis of permeable pavement hydrological modelling in the Storm Water Management Model, J. Hydrol. 600 (2021) 126525, http://dx.doi.org/10.1016/j.jhydrol.2021.126525.

[21] M. Radwan, P. Willems, J. Berlamont, Sensitivity and uncertainty analysis for river quality modelling, J. Hydroinform. 6 (2) (2004) 83–99, http://dx.doi.org/10.2166/hydro.2004.0008.

[22] N. Bateni, S.H. Lai, F.J. Putuhena, D.Y.S. Mah, M.A. Mannan, R.J. Chin, Hydrological impact assessment on permeable road pavement with subsurface precast micro-detention pond, Water Environ. J. 34 (S1) (2020) 960–969, http://dx.doi.org/10.1111/wej.12613.

[23] S. Gülbaz, C.M. Kazezyılmaz-Alhan, An evaluation of hydrologic modeling performance of EPA SWMM for bioretention, Water Sci. Technol. 76 (11) (2017) 3035–3043, http://dx.doi.org/10.2166/wst.2017.464.

[24] M. Turco, R. Kodešová, G. Brunetti, A. Nikodem, M. Fér, P. Piro, Unsaturated hydraulic behaviour of a permeable pavement: Laboratory investigation and numerical analysis by using the HYDRUS-2D model, J. Hydrol. 554 (2017) 780–791, http://dx.doi.org/10.1016/j.jhydrol.2017.10.005.

[25] DHI, Estudio de Actualización del Análisis de Las Precipitaciones Intensas y Recomendaciones de Cálculo de Caudales de Avenidas en Pequeñas Cuencas del Territorio Histórico de Gipuzkoa, Technical Report, Gipuzkoako Foru Aldundia, 2018.

[26] A. Freire Diogo, J. Antunes do Carmo, Peak flows and stormwater networks design—current and future management of urban surface watersheds, Water 11 (4) (2019) http://dx.doi.org/10.3390/w11040759.
[27] A. Palla, I. Gnecco, M. Carbone, G. Garofalo, L. Lanza, P. Piro, Influence of stratigraphy and slope on the drainage capacity of permeable pavements: laboratory results, Urban Water J. 12 (5) (2014) 394–403, http://dx.doi.org/10.1080/1573062X.2014.900091.
[28] B. Woods Ballard, S. Wilson, H. Udale-Clarke, S. Illman, R. Ashley, R. Kellagher, The SUDS Manual, CIRIA, London, 2015.
[29] P.T. Weiss, M. Kayhanian, J.S. Gulliver, L. Khazanovich, Permeable pavement in northern North American urban areas: research review and knowledge gaps, Int. J. Pavement Eng. 20 (2) (2019) 143–162, http://dx.doi.org/10.1080/10298436.2017.1279482.
[30] D.R. Smith, D.K. Hein, Development of a national ASCE standard for permeable interlocking concrete pavement, in: Green Streets, Highways, and Development 2013: Advancing the Practice, American Society of Civil Engineers (ASCE), 2013, pp. 89–105, http://dx.doi.org/10.1061/9780784413197.008.
[31] J. Hou, Y. Zhang, Y. Tong, K. Guo, W. Qi, R. Hinkelmann, Experimental study for effects of terrain features and rainfall intensity on infiltration rate of modelled permeable pavement, J. Environ. Manag. 243 (2019) 177–186, http://dx.doi.org/10.1016/j.jenvman.2019.04.096.
[32] F. Alonso López, Accesibilidad en Los Espacios Públicos Urbanizados, Ministerio de Vivienda, Gobierno de España, 2010.
[33] L.M. Tallaksen, A review of baseflow recession analysis, J. Hydrol. 165 (1) (1995) 349–370, http://dx.doi.org/10.1016/0022-1694(94)02540-R.
[34] J. Sujono, S. Shikasho, K. Hiramatsu, A comparison of techniques for hydrograph recession analysis, Hydrol. Process. 18 (3) (2004) 403–413, http://dx.doi.org/10.1002/hyp.1247.
[35] L.A. Rossman, W.C. Huber, Storm Water Management Model Reference Manual, 2016.
[36] E. Madrazo-Uribeetxebarria, M. Garmendia Antín, J. Almandoz Berrondo, I. Andrés-Doménech, Modelling runoff from permeable pavements: a link to the curve number method, Water 15 (1) (2022) 160, http://dx.doi.org/10.3390/w15010160.
[37] J.E. Nash, J.V. Sutcliffe, River flow forecasting through conceptual models part I — A discussion of principles, J. Hydrol. 10 (3) (1970) 282–290, http://dx.doi.org/10.1016/0022-1694(70)90255-6.
[38] K. Mullen, D. Ardia, D. Gil, D. Windover, J. Cline, DEoptim: An R package for global optimization by differential evolution, J. Stat. Softw. 40 (6) (2011) 1–26, http://dx.doi.org/10.18637/jss.v040.i06.
[39] R Core Team, R: A Language and Environment for Statistical Computing, R Foundation for Statistical Computing, Vienna, Austria, 2021.
[40] J. Huang, J. He, C. Valeo, A. Chu, Temporal evolution modeling of hydraulic and water quality performance of permeable pavements, J. Hydrol. 533 (2016) 15–27, http://dx.doi.org/10.1016/j.jhydrol.2015.11.042.
[41] E.Z. Bean, W.F. Hunt, D.A. Bidelspach, Evaluation of four permeable pavement sites in eastern North Carolina for runoff reduction and water quality impacts, J. Irrig. Drain. Eng. 133 (6) (2007) 583–592, http://dx.doi.org/10.1061/(ASCE)0733-9437(2007)133:6(583).
[42] B.O. Brattebo, D.B. Booth, Long-term stormwater quantity and quality performance of permeable pavement systems, Water Res. 37 (18) (2003) 4369–4376, http://dx.doi.org/10.1016/S0043-1354(03)00410-X.